POLAR CO_2 ICE CLOUDS AND ENERGY BUDGET FROM MARS CLIMATE SOUNDER DATA

P. O. Hayne, D. J. McCleese, W. A. Abdou, D. M. Kass, A. Kleinböhl, T. McDunn, S. Piqueux, J. H. Shirley, J. T. Schofield, and the MCS Team, *Jet Propulsion Laboratory/California Institute of Technology, Pasadena, California, USA (Paul.O.Hayne@jpl.nasa.gov).*

Background:

Polar carbon dioxide snow clouds were predicted on Mars at least as early as the 1960's on the basis of theoretical calculations [Gierasch and Goody, 1968], and modern spacecraft observations have confirmed their common occurrence during polar night in both hemispheres [Neumann *et al.*, 2003]. Mars general circulation models (GCMs) now commonly incorporate a CO_2 snowfall scheme based on cloud microphysical and sedimentation models to simulate the past and present climate [e.g. Forget *et al.*, 1998; Kuroda *et al.*, 2013]. However, observational constraints on this process and its consequences for the Martian climate are sparse.

If snow particles reach the surface, they may contribute substantial material to the seasonal caps of Mars, in addition to direct surface frost formation. Snow clouds also affect the planetary heat budget through two primary mechanisms: 1) snow particles decrease polar infrared emissivity during winter, and 2) fine-grained snow deposits may increase polar cap albedo during summer. These effects may strongly alter the seasonal cap mass budget, and possibly explain the existence of the perennial CO_2 deposits near the Martian south pole. Mapping the distribution and quantifying the abundance of CO_2 snowfall therefore have important implications for the study of Mars' present-day climate.

Instrument and Dataset:

We used data from the Mars Climate Sounder (MCS) in order to retrieve CO_2 cloud opacity and surface properties within the polar winter regions during four Mars years. MCS is a passive 9-channel radiometer on the Mars Reconnaissance Orbiter (MRO) that is optimized for atmospheric observations, but that also acquires surface information [McCleese *et al.,* 2007]. The instrument consists of two telescopes that are designed to be slewed in azimuth and elevation to view the martian atmosphere in limb, nadir, and on-planet geometries. Each channel consists of 21 vertically-oriented detectors, which acquire simultaneous radiance measurements from the surface up to ~80 km. Their angular separation provides an altitude resolution of ~5 km at the Mars limb.

MCS has 8 mid- and far-infrared channels and one visible/near-IR channel, covering 0.3 to 45 µm. Three channels cover frequencies around the 15 µm CO_2 absorption band (A1, A2 and A3) and are used for pressure and temperature sounding. A channel centered around 22 µm (A5) gives information about dust opacity while a channel centered at 12 µm (A4) covers an absorption feature of water ice. In the far-IR three channels (B1, B2, and B3) are designed to give information about surface temperature, water vapor abundance and dust and condensate opacities. Kass *et al.* [2014] describe other aspects of this dataset in more detail.

Although CO_2 ice was not included in earlier versions of the MCS retrieval algorithm, we have begun implementing this component for future releases. Currently, the CO_2 ice opacity retrievals typically use the 22-µm (A5) channel, although future versions of the algorithm will instead utilize either the 16.5-µm (A1) or 32-µm (B1) channel to distinguish CO_2 ice from dust.

Temperature Profiles and Cloud Formation:

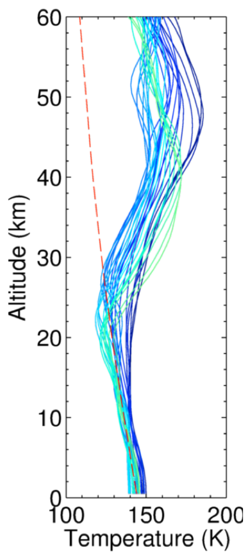

Figure 1: MCS south polar winter temperature profiles (dashed line = condensation temperature)

In the martian polar night, the atmosphere and ground may cool to the local CO_2 condensation temperature, due to a lack of sunlight and the resulting surplus of infrared radiation to space. Gierasch and Goody [1968] showed that nighttime formation and vertical propagation of CO_2 clouds is likely to occur within the polar regions due to infrared cooling alone. Once the atmosphere is actively condensing, temperatures should remain very close to the frost point due to the release of latent heat. Figure 1 shows that this is a typical situation in retrieved MCS polar temperature profiles. Within the polar night, temperatures are most often within ~5 K of the local condensation temperature at altitudes < 20 km, and sometimes show high amounts of supersaturation [Hu *et al.*, 2012]. At latitudes near the edge of polar night, diurnal temperature variations are observed, and daytime CO_2 clouds have not so far been identified in these regions.

Polar Cloud Composition and Particle Size: Polar winter atmospheric reflections recorded by the Mars Orbiter Laser Altimeter (MOLA) occur where CO_2 clouds could form based on temperature [Hu *et al.*, 2012], but the measurement lacks definitive compositional information [Colaprete *et al.*, 2003]. We used multi-spectral radiance profiles from MCS to distinguish CO_2 ice clouds from other possible aerosols [Hayne *et al.*, 2012]. Our radiative transfer "forward" model incorporates Mie scattering parameters for water ice and dust as in Kleinbohl *et al.* [2011] and for CO_2 ice particles of varying sizes using optical constants from Hansen [1997].

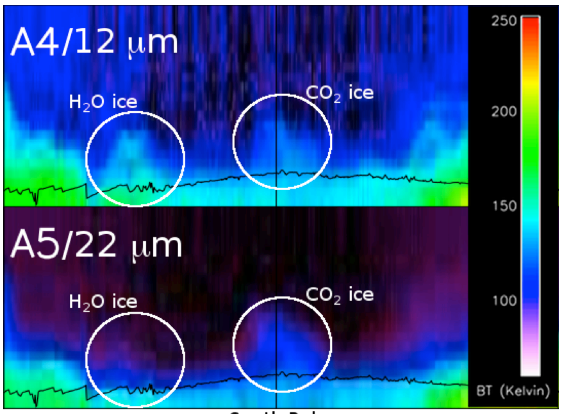

Figure 2: Polar cloud brightness temperature profiles from MCS. The vertical axis is detector # (i.e. altitude) and the horizontal axis plots time along the polar orbit.

Through iterative relaxation [Chahine, 1972; Kleinbohl *et al.*, 2009], we fit the MCS radiance data to retrieve aerosol opacity profiles. Among the diverse compositions investigated, only CO_2 ice particles in the size range 10–100 μm yielded a proper fit in all spectral bands [Hayne *et al.*, 2012]. This distinct composition can be seen in the brightness temperature data, in which CO_2 ice clouds appear equally bright at both 12 and 22 μm, whereas water ice layers are nearly transparent at the longer wavelength (Fig. 2).

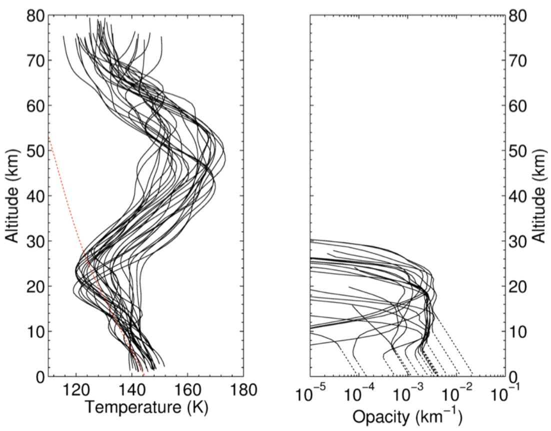

Figure 3: Retrieved temperature and opacity profiles in the south polar region, Ls = 89.5°, MY29 (June 24, 2008). [Hayne et al.*, 2013a]*

Retrieved CO_2 ice opacity profiles show good agreement with retrieved temperature profiles (Fig. 3), although retrieval success is significantly lower in the dusty northern winter. Typical cloud infrared optical depths of ~0.01-0.1 occur near both poles during winter, although cloud opacity at altitudes < 4 km is more uncertain due to contamination by surface emission. MCS may also record clouds with total normal optical depths > 0.1, but in this case the cloud is optically thick along the line of sight and the retrieval is cut off. The CO_2 clouds occur at altitudes < 30 km within the polar vortex, with cloud height and optical depth increasing toward the pole. Occasionally detached layers of CO_2 ice are observed (usually near ~20 km), but most clouds increase in opacity toward the surface.

Cooling and Snowfall Rate Calculations: We developed two models to constrain snowfall rates based on MCS south polar cloud observations [Hayne *et al.*, 2013a]: 1) a radiative cooling model including infrared absorption and emission by observed aerosols and gaseous CO_2, and 2) a cloud sedimentation model including atmospheric turbulence. Cooling rates can be converted to snowfall rates by integrating over the column:

$$\frac{dm}{dt} \sim \frac{c_p}{L}\int_0^\infty \left(\rho \frac{dT}{dt}\right) dz,$$

where m is the mass of snow per unit area, ρ and c_p are the density and heat capacity of the atmosphere, and L is the latent heat of CO_2 deposition (~$5.9\text{x}10^5$ J/kg). We calculate dT/dt directly from the retrieved opacity, temperature, and pressure profiles. Neglecting meridional heat advection, the observations are consistent with a snowfall mass deposition rate up to ~$4.2\text{x}10^{-5}$ kg/m^2/s, or ~20% of the total material. If advected heat corresponds to the typical ~2 W/m^2 from Pollack *et al.* [1990], the snowfall accounts for < 6% of the total.

Snowfall rates determined from sedimentation model calculations are similar: 0.05–15% of the total condensed carbon dioxide at the surface. We found that these results were not sensitive to the eddy viscosity of the atmosphere, which only affected the time-dependent vertical structure of the cloud. The precipitation rates determined by the two models most closely matched if snow particles were in the size range 30–100 μm. This size range is also consistent with the apparent fallout of clouds on the MRO orbital time scale of ~2 hr, which requires particles > 50 μm.

Hemispheric Comparisons: Excellent wintertime coverage of the MCS dataset over both poles allows direct comparisons of

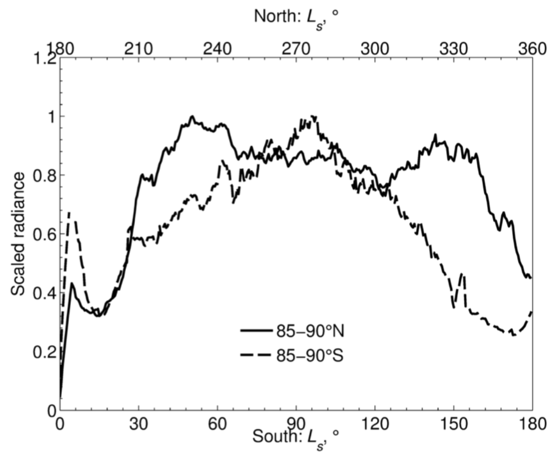

Figure 4: Comparison of polar cloud activity in the two martian hemispheres over MY28-MY31, using mean MCS 32-µm radiance as a proxy for cloud optical depth.

CO_2 cloud properties and behavior. Successful retrievals are more limited in the northern hemisphere due to greater dust activity in its winter season. We therefore used channel B1 (32 µm) scaled radiance values at 10-20 km altitude as a proxy for cloud activity (cf. Fig. 2), which allows rapid analysis of multiple Mars years of data. Figure 4 shows that clouds occur in distinct patterns in the two hemispheres: single-peaked in the south, and double-peaked in the north. The bimodal behavior in the northern hemisphere is due to the annual dust storms initiated in southern summer, which generate excess dynamical heating due to subsidence and disruption of the north polar vortex [Hayne *et al.*, 2013b, Kass *et al.*, 2013]. In contrast, in the south CO_2 cloud activity is driven primarily by radiative cooling, and closely follows the region of polar night.

Tropospheric condensation of CO_2 is much more spatially confined in the northern hemisphere, occurring primarily at latitudes > 70°N, compared to southern hemisphere activity > 60°S. We attribute this to the smaller extent of the northern polar winter vortex. However, where clouds occur in the north, they occur with much greater frequency than in the south.

Inter-annual Comparisons:

The MCS dataset now spans four Mars years (MY28–MY31), allowing direct inter-annual comparisons of CO_2 cloud activity and the radiation budget. Although measurable variations occurred, cloud activity and polar cap infrared emissivity patterns are remarkably repeatable. For example, the bimodal distribution of polar clouds over the northern polar winter season repeats each year with approximately the same amplitude, with the possible exception of MY28, when a global dust storm occurred.

We compared MCS nadir-viewed brightness temperatures with retrieved polar cloud optical depth (or limb radiance as a proxy). In MY29 late northern winter cloud activity was significantly lower than the two adjacent years, likely due to increased dust storm activity. As shown in Fig. 5, we also observe a significant increase in surface emissivity in MY29, potentially linking snowfall activity to the surface thermal emission.

Surface emissivity is also correlated with cloud activity in the southern hemisphere, as manifested in MY31, when mid-winter clouds were especially persistent and surface emissivity was significantly lower than the average. The reverse situation occurred in MY30, when cloud activity was low.

Effects on Polar Energy Budget:

At the low surface elevations of the northern plains of Mars, equilibrium CO_2 frost temperatures are ~5–10 K higher than in the south, which should lead to greater thermal emission as long as the

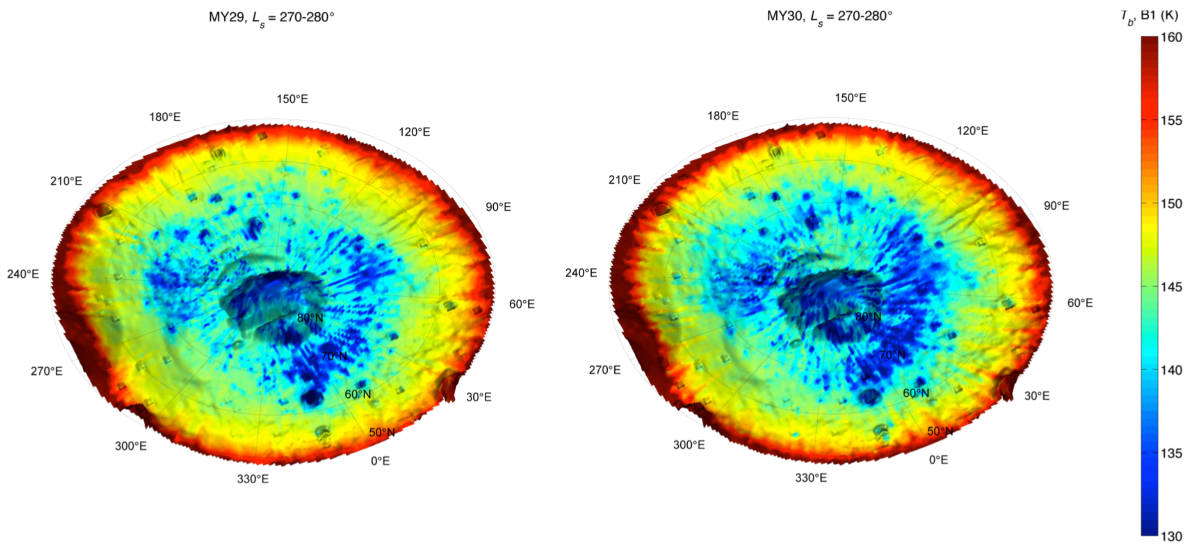

Figure 5: MCS north polar nadir brightness temperatures at 22 µm, with blues and greens indicating low-emissivity “cold spots” associated with fine-grained CO_2 snow deposits. Note the significant reduction in cold spots in MY29 (left), when cloud activity was lower than average.

ground is frost-covered. However, the MCS data show that the spatially- and spectrally-integrated infrared flux remains nearly the same at both poles over their winter seasons. In this case, the net accumulation of CO_2 frost is given by a balance between outgoing long-wave radiation and the latent heat of deposition, such that:

$$M \sim \langle F_{IR} \rangle \Delta t / L$$

where the quantity in brackets is the mean broadband IR flux, and Δt is the length of the polar winter season. Because their observed IR fluxes are the same, the ratio of wintertime mass accumulation at the two poles is then just the ratio of the lengths of their winters: $\Delta t_s / \Delta t_n \approx 1.15$, i.e. we expect ~15% greater accumulation at the south pole during winter. The summertime cap albedo and conduction into the subsurface also strongly affect the annual mass balance of CO_2 between the polar caps and atmosphere, again probably favoring the south pole for net accumulation [Paige and Ingersoll, 1985; Jakosky and Haberle, 1990].

Conclusions and Future Work:

Infrared sounding by the Mars Climate Sounder over four Mars years (MY28–MY31) shows a repeatable pattern of polar winter CO_2 cloud activity, with significant differences between the two poles. South polar cloud opacity correlates strongly with the extent of polar night, indicating control by radiative cooling. In the north, cloud activity is suppressed near mid-winter due to disruption of the polar vortex by annual dust storm activity originating in the southern hemisphere. Carbon dioxide snowfall composed of particles ~10–100 μm in radius contributes ~3–20% by mass to the growing south polar seasonal cap, consistent with earlier GCM results [Forget *et al.*, 1998].

Inter-annual differences observed by MCS show that decreased CO_2 snow cloud activity is correlated with increased effective infrared emissivity of the polar caps, consistent with the radiative properties of granular carbon dioxide ice [Hayne *et al.*, 2012; Hansen, 2013]. Overall, the northern seasonal cap has lower emissivity, leading to greater expected wintertime accumulation of CO_2 ice at the south pole.

A modified version of the MCS retrieval algorithm including CO_2 ice retrievals has been tested and validated, and will be included in a future release.

References: Chahine (1972), *J. Atmos. Sci., 29;* Colaprete *et al.* (2003), *JGR, 108 (E7)*, 5081, doi:10.1029/2003JE002053*;* Forget *et al.* (1998), *Icarus*, *131*, 302–316; Hansen (1997), *JGR, 102*(E9), 21569–21587, doi:10.1029/97JE01875; Hayne *et al.* (2012), *JGR, 117,* doi:10.1029/2011JE004040; Gierasch and Goody (1968), *Planet. Space Sci., 16*, 615–646; Hayne *et al.* (2013a), *Icarus*, in press, doi:10.1016/j.icarus.2013.10.020; Hayne *et al.* (2013b), *AGU Fall Mtg.*, #P41C-1934; Hu *et al.* (2012), *JGR*, *117*, E07002, doi:10.1029/2012JE004087; Jakosky and Haberle (1990), *JGR, 95*(B2), 1359–1365; Kass *et al.* (2013), *AGU Fall Mtg.*, #P32A-07; Kass *et al.* (2014), *Fifth Int. Workshop on the Mars Atmos.*, this volume; Kleinböhl *et al.* (2009), *JGR 114*, E10006, doi:10.1029/2009JE003358; Kleinböhl *et al.* (2011), *JQRST, 112*, 1568-1580; Kuroda *et al.* (2013), *GRL*, *40*, 1484–1488, doi:10.1002/grl.50326; McCleese *et al.* (2007), *JGR, 112,* E05S06 doi: 10.1029/2006JE002790; Neumann *et al*. (2003), *JGR*, *108*, E4/5023, doi: 10.1029/2002JE001849; Paige and Ingersoll (1985), *Science, 228*, 1160–1168; Pollack *et al.* (1990), *JGR, 95*, 1447–1473

Acknowledgement: This work was carried out at the Jet Propulsion Laboratory, California Institute of Technology under a contract with the National Aeronautics and Space Administration.